

PERFORMANCE ANALYSIS OF STAR FOR CELLULAR CDMA SYSTEMS

Weigang Li, Sofiène Affes, and Paul Mermelstein

INRS-Télécommunications

Université du Québec, Canada

16, Place du Commerce, Ile-des-Soeurs, Quebec, H3E 1H6

Tel: (514) 761-8636 - Fax: (514) 761-8501

e-mail: wli@inrs-telecom.quebec.ca

Abstract

In this contribution, we present a performance analysis of STAR, the spatio-temporal array-receiver for cellular CDMA systems. First, we perform a convergence analysis and provide the stability condition, the steady-state misadjustment and the speed of the identification step. From these results, we compute the probability of false detection of the time-delay acquisition step. Next, we study their impact on both the acquisition and the tracking modes and give analytical expressions for the output signal to noise ratio (SNR) and capacity. Finally, we confirm by simulations the performance analysis and the enhancements achieved by STAR in acquisition and capacity.

1. Introduction

Array processing was recently applied to CDMA systems to improve the capacity of personal communication systems [1],[2]. Its exploitation motivates the development of new CDMA array-receivers combining acquisition. These techniques involve processing both in time for synchronization, and in space for combining multiple diversity branches.

Recently, a spatio-temporal array-receiver (STAR) using a new space/time structural approach was proposed [3],[4]. Compared to previous methods (*e.g.*, 2D-RAKE [5], RAKE-like [6]), STAR offers many advantages such as an attractive formulation, very low complexity and high performance.

In this paper we provide a theoretical performance analysis of STAR and validate it by simulations.

2. Signal Model and Algorithm

We consider a cellular CDMA system where each base station is equipped with a receiving antenna of M sensors. The BPSK bit sequence of the desired user is

The work reported here was supported by the Bell Quebec/NORTEL/NSERC Industrial Research Chair in Personal Communications

first differentially encoded at the rate $1/T$ where T is the bit duration. The resulting DBPSK sequence $b(t)$ is then spread by a personal and periodic code $c(t)$ with period T at the rate $1/T_c$ where T_c is the chip pulse duration. The processing gain is then given by $L = T/T_c$. A multipath fading environment with a number of paths P is also assumed.

At time t , the $M \times 1$ observation vector received by the antenna array is written as:

$$X(t) = \psi(t) \sum_{p=1}^P G_p(t) \varepsilon_p(t) b(t - t_p) c(t - t_p) + I(t), \quad (1)$$

where $t_p \in [0, T)$ are the propagation time-delays, $G_p(t)$ are the normalized propagation vectors, $\varepsilon_p^2(t)$ are the fractions of the total power $\psi^2(t)$ received from the desired user along each path. $I(t)$ is the noise term which includes the thermal noise received at the antenna elements as well as the self, in-cell, and out-cell interference.

We make the reasonable assumption that the time variations of $G_p(t)$, $\varepsilon_p^2(t)$, and $\psi^2(t)$ are slow and locally constant as compared to the bit duration T . To keep the discussion simple, we also assume that the time-delays are constant in time and equal to multiples of the chip duration T_c (*i.e.*, $t_p \simeq \tau_p T_c$, s.t. $\tau_p \in \{0, \dots, L - 1\}$). Time-delay tracking with STAR is specifically addressed in [3]. For the need of the analysis, we make further assumptions as follows:

- the interference is a spatially and temporally white Gaussian process with mean zero and variance σ_I^2 ,
- the number of paths P is perfectly known,
- a perfect power control is achieved (*i.e.*, $\psi(t)^2 = \psi^2$).

After despreading and sampling of $X(t)$ at the chip rate, the resulting stream of data, say $Z(t)$, can be sliced at the bit rate into compact matrices following the post-correlation model (PCM) developed in [3]:

$$\mathbf{Z}_n = s_n \mathbf{H}_n + \mathbf{N}_n, \quad (2)$$

where $s_n = \psi_n b_n$ is the signal component, and \mathbf{Z}_n is the $M \times L$ post-correlation data matrix whose columns

are $Z_n(k) = Z(nT + kT_c)$ for $k = 0, \dots, L-1$. The $M \times L$ noise matrix \mathbf{N}_n , with variance $\sigma_N^2 = \sigma_I^2/L$ at each element, results from the despreading and sampling of interference. The columns of the $M \times L$ propagation matrix \mathbf{H}_n , denoted by $H_n(k)$, are modeled in [3] as:

$$H_n(k) = \sum_{p=1}^P G_{p,n} \varepsilon_{p,n} \rho(k - \tau_p) \quad (3)$$

$$\simeq \begin{cases} \varepsilon_{p,n} G_{p,n} & \text{if } k = \tau_p \text{ for } p = 1, \dots, P, \\ 0 & \text{if } k \neq \tau_p, \end{cases}$$

where $\rho(k)$ is the auto-correlation function of the chip pulse. Since τ_p is an integer, we use the approximation $\rho(k - \tau_p) \simeq \delta(k - \tau_p)$. To avoid the ambiguity due to a multiplicative factor between \mathbf{H}_n and s_n , we fix the norm of \mathbf{H}_n at \sqrt{M} (i.e., $\|G_{p,n}\|^2 = M$). By reshaping the $M \times L$ matrices in Eq. (2) into $ML \times 1$ spatio-temporal vectors, we obtain the following narrowband version of the PCM model [3]:

$$\mathbf{Z}_n = s_n \mathbf{H}_n + \mathbf{N}_n, \quad (4)$$

where \mathbf{Z}_n , \mathbf{H}_n and \mathbf{N}_n denote the resulting vectors. Eq. (4) shows that the desired signal lies in a one-dimensional spatio-temporal signal subspace. Therefore, it allows an efficient use of simple narrowband array processing techniques [3].

Indeed, at each block iteration, an estimate of \mathbf{H}_n , say $\hat{\mathbf{H}}_n$, is provided by STAR. Then, by narrowband matched beamforming [3], s_n , b_n and ψ_n are first estimated as follows:

$$\hat{s}_n = \text{Re}\{\hat{\mathbf{H}}_n^H \mathbf{Z}_n / M\} = \sum_{k=0}^{L-1} \text{Re}\{\hat{H}_n(k)^H Z_n(k) / M\}, \quad (5)$$

$$\hat{b}_n = \text{sign}\{\hat{s}_n\}, \quad (6)$$

$$\hat{\psi}_n^2 = (1 - \alpha) \hat{\psi}_{n-1}^2 + \alpha \hat{s}_n^2, \quad (7)$$

where α is a smoothing factor. Second, the channel estimate $\hat{\mathbf{H}}_n$ is updated in a decision feedback identification (DFI) scheme, by feeding back the signal component estimate \hat{s}_n as a reference signal in the following LMS-type eigen-subspace tracking procedure [3]:

$$\hat{\mathbf{H}}_{n+1} = \hat{\mathbf{H}}_n + \mu \left(\mathbf{Z}_n - \hat{\mathbf{H}}_n \hat{s}_n \right) \hat{s}_n, \quad (8)$$

where μ is an adaptation step-size. This DFI scheme allows a 3 dB coherent detection gain in noise reduction in Eq. (5) by recovering the channel phase offsets in Eq. (8) without a pilot [3].

After convergence, we define, for $k = 0, \dots, L-1$, a localization spectrum which simplifies from [3] to:

$$\hat{S}_n^2(k) = D(k)^H \hat{\mathbf{H}}_n^H \hat{\mathbf{H}}_n D(k) = \|\hat{H}_n(k)\|^2, \quad (9)$$

where $D(k)$ is an $L \times 1$ vector which is null except for the $(k+1)$ th component which is equal to 1. It approximates the following perfect localization spectrum:

$$S_n^2(k) = \|H_n(k)\|^2 \quad (10)$$

$$= \begin{cases} \varepsilon_{p,n}^2 M & \text{if } k = \tau_p \text{ for } p = 1, \dots, P, \\ 0 & \text{if } k \neq \tau_p, \end{cases}$$

Since P is assumed to be known, the time-delays can be estimated as the values $\hat{\tau}_p$ of $k \in \{0, \dots, L-1\}$ for which $\hat{S}_n^2(k)$ displays the P largest peaks. In the tracking mode, Eq. (5) finally simplifies from [3] to:

$$\hat{s}_n = \sum_{p=1}^P \text{Re}\left\{ \hat{H}_n(\hat{\tau}_p)^H Z_n(\hat{\tau}_p) / M \right\}. \quad (11)$$

As mentioned earlier, the tracking of the time-delays and their number is addressed in [3].

3. Performance Analysis

In this analysis, we first study the convergence of the identification procedure of Eq. (8). Secondly, we assess its effect on time-delay acquisition of Eq. (9). Finally, we evaluate the impact of both identification and time-delay acquisition errors on the output SNR and the capacity in the tracking mode of Eq. (11).

3.1. Accuracy of Channel Identification

We study the accuracy of the channel identification step in terms of the speed of acquisition and the mean square error (MSE) of channel identification errors.

To simplify the analysis, we make the approximation that $\hat{s}_n = s_n$. We will see next that this approximation is reasonable at relatively low input SNR values. The DFI scheme of Eq. (8) reduces in this case to an exact adaptive LMS implementation¹ whose analysis can be made following well-known methodologies explained in [7].

First, we easily prove that the propagation matrix estimator \mathbf{H}_n is asymptotically unbiased. Second, if we denote by $\beta_{m,k}^2(n)$ the identification MSE over the (m, k) th component of the $M \times L$ propagation matrix \mathbf{H}_n , then we obtain the following recursion:

$$\beta_{m,k}^2(n) \simeq (1 - \mu\psi^2)^{2n} \beta_{m,k}^2(0) + \mu\sigma_N^2 \frac{1 - (1 - \mu\psi^2)^{2n}}{2 - \mu\psi^2}, \quad (12)$$

where $\beta_{m,k}^2(0)$ is the initial MSE. Based on this equation, we obtain the *stability condition* for convergence:

$$0 < \mu < \mu_{\max} = \frac{2}{\psi^2}, \quad (13)$$

¹A further study involving the DFI scheme of Eq. (8) effectively implemented in STAR is under way.

the *time constant* to convergence:

$$n_{cv} = \frac{1}{2\mu\psi^2}, \quad (14)$$

and the *steady-state misadjustment* at convergence:

$$\beta^2 = \lim_{n \rightarrow \infty} \frac{E \left[\|\mathbf{H}_n - \hat{\mathbf{H}}_n\|^2 \right]}{ML} = \frac{\mu}{\mu_{\max} - \mu} \frac{1}{SNR_{in}}, \quad (15)$$

where $SNR_{in} = \psi^2/\sigma_N^2$ is the input SNR after despreading, all regardless of the index pair (m, k) .

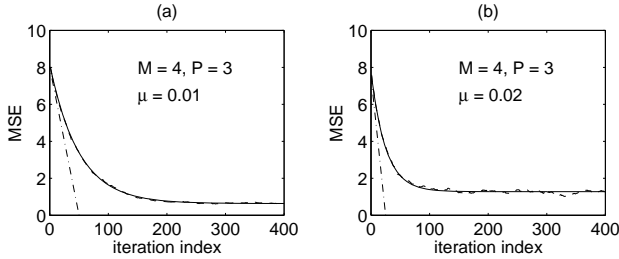


Figure 1 Total identification MSE $ML\beta^2(n)$ versus the iteration index n at an input SNR of 3 dB for different values of μ : theoretical (solid), experimental (dashed), slope of convergence (semi-dashed).

Fig. 1 shows the theoretical and experimental learning curves with two practical values of μ in the stability range of Eq. (13), typically small compared to the upper bound μ_{\max} . They confirm that the speed of convergence can be made as fast as required with higher values of μ . As expected from Eq. (14), we can measure from the initial slopes of the curves that the constant time n_{cv} is equal to 50 and 25 with μ fixed at 0.01 and 0.02 respectively. With $\mu = 0.05$ as in [3],[4], convergence is reached in a time interval as short as 10 bit iterations. This is also the time required for time-delay synchronization. Therefore, STAR achieves very fast acquisition.

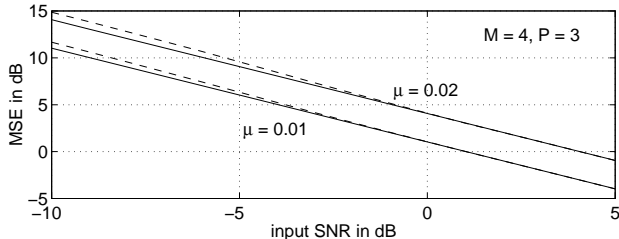


Figure 2 Total identification MSE at steady state $ML\beta^2$ in dB versus the input SNR after despreading for different values of μ : theoretical (solid), experimental (dashed).

Notice however that the steady-state misadjustment increases with higher values of μ , showing a trade-off

between the acceleration of acquisition and the reduction of identification errors. Fig. 2 shows a 3 dB increase in identification MSE as we double the step-size value μ . As expected from Eq. (15), it also shows that identification errors decrease linearly with the input SNR on a dB scale. Notice finally that the experimental and theoretical curves become closer and almost coincide as the SNR values increase, thereby confirming that the approximation $\hat{s}_n = s_n$ becomes reasonable at relatively low SNR values.

By controlling the steady-state misadjustment, the selection of μ has an additional effect on time-delay acquisition other than fixing the speed of synchronization. It also determines the quality of acquisition. To illustrate this effect, we can see that the localization spectrum of Eq. (9) has the following average value:

$$E \left[\hat{S}_n^2(k) \right] = M \left(\sum_{p=1}^P \varepsilon_{p,n}^2 \delta(k - \tau_p) + \beta^2 \right). \quad (16)$$

The above-mentioned trade-off between speed and misadjustment thus translates into a more interesting trade-off between speed and accuracy of time-delay acquisition that we evaluate next in more detail.

3.2. Accuracy of Time-Delay Acquisition

We assess the accuracy of time-delay acquisition in terms of probability of false detection (*i.e.*, at least one path was not detected). To do so, we define the event of a correct acquisition of all paths:

$$\begin{aligned} \mathcal{A} &= \left\{ \min_{p=1, \dots, P} \left\{ \hat{S}_n(\tau_p) \right\} > \max_{k \notin \{\tau_1, \dots, \tau_P\}} \left\{ \hat{S}_n(k) \right\} \right\} \quad (17) \\ &= \bigcap_{\substack{p=1, \dots, P \\ k \notin \{\tau_1, \dots, \tau_P\}}} \left\{ \hat{S}_n(\tau_p) > \hat{S}_n(k) \right\} = \bigcap_{\substack{p=1, \dots, P \\ k \notin \{\tau_1, \dots, \tau_P\}}} \mathcal{A}(\tau_p, k). \end{aligned}$$

The probability of $\mathcal{A}(\tau_p, k) = \left\{ \hat{S}_n(\tau_p) > \hat{S}_n(k) \right\}$ is given by:

$$p_c(\tau_p, k) = \mathcal{P} [\mathcal{A}(\tau_p, k)] = \int_0^{+\infty} \int_0^x f_{\tau_p, k}(x, y) dx dy, \quad (18)$$

where $f_{\tau_p, k}(x, y)$ is the joint probability density function of $\hat{S}_n(\tau_p)$ and $\hat{S}_n(k)$. The positive random variables $\hat{S}_n(\tau_p)$ and $\hat{S}_n(k)$ have respectively a Ricean and a generalized Rayleigh distribution [8] with probability density functions given over $[0, +\infty)$ by:

$$f_{\tau_p}(x) = \frac{2x^M B_{M-1} \left(\frac{2\sqrt{M}\varepsilon_{p,n}x}{\beta^2} \right)}{\beta^2 (\sqrt{M}\varepsilon_{p,n})^{M-1}} e^{-\frac{x^2 + M\varepsilon_{p,n}^2}{\beta^2}}, \quad (19)$$

$$f_k(x) = \frac{2x^{2M-1}}{\beta^{2M} \Gamma(M)} e^{-\frac{x^2}{\beta^2}}, \quad (20)$$

where Γ is the Gamma function and B_i is the i th-order modified Bessel function of the first degree. We assume here that $\hat{S}_n(\tau_p)$ and $\hat{S}_n(k)$ are independent. Therefore, $p_c(\tau_p, k)$ is constant for $k \notin \{\tau_1, \dots, \tau_P\}$ and given by:

$$p_c(\tau_p, k) = p_c(\tau_p) = \int_0^{+\infty} \int_0^{+\infty} f_{\tau_p}(x) f_k(y) dx dy. \quad (21)$$

From Eq. (17) and Eq. (21), we obtain the probability of false detection as:

$$p_f = 1 - \mathcal{P}[A] = 1 - \prod_{\substack{p=1, \dots, P \\ k \notin \{\tau_1, \dots, \tau_P\}}} p_c(\tau_p, k) = 1 - \prod_{p=1}^P p_c(\tau_p)^{(L-P)} \quad (22)$$

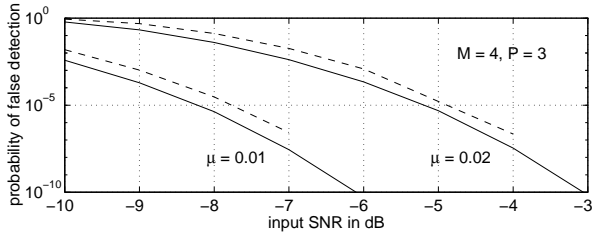


Figure 3 Probability of false detection p_f versus the input SNR after despreading for different values of μ : theoretical (solid), experimental (dashed).

In Fig. 3, we plot the experimental and theoretical curves of p_f obtained by numerical computation using, respectively, the experimental and theoretical values of β^2 given in Fig. 2 and assuming an equal power partition over paths (*i.e.*, $\varepsilon_{p,n}^2 = 1/P$). Both curves show that p_f is extremely small at relatively very low SNR values. In this range of SNR, the gap between the theoretical and experimental misadjustments of Fig. 2 produces a factor of almost 10 between the theoretical and experimental probabilities of false detection. This factor should decrease to 1 at higher SNR values untested here due to computational accuracy limitations.

As we double the step-size value μ , notice that we translate the curve by 3 dB in input SNR. With $M = 4$ antennas and $P = 3$ equal power paths, we can expect at an input SNR around 0 dB an experimental probability of false detection as small as $p_f \simeq 10^{-6}$ with $\mu = 0.05$. With this value of μ , time-delay acquisition is made within 10 bit iterations only. Therefore, STAR can achieve very fast synchronization with a very small probability of false detection.

3.3. Impact on SNR and Capacity

We assess now the impact of identification and acquisition errors on the system capacity, the key figure in

performance results. For the sake of simplicity, we do not consider the case of a dynamic capacity but estimate the maximum number of users accommodated in the tracking mode given a required bit error rate (BER).

To do so, we need the output SNR in the tracking mode, but we also provide the output SNR in the acquisition mode for comparison. Following the same methodology as in [4], we derive both expressions using Eq. (11) and Eq. (5) respectively, along with Eq. (15). First, at the acquisition mode, the output SNR is:

$$SNR_{\text{out}}^A = SNR_{\text{in}} \frac{2M}{\frac{\mu(\sigma_f^2 + \psi^2)}{2 - \mu\psi^2} + 1}. \quad (23)$$

Second, at the tracking mode, the output SNR is:

$$SNR_{\text{out}}^T = \sum_{\bar{P}=0}^P p_f(\bar{P}) SNR_{\text{out}}^{(\bar{P})}, \quad (24)$$

where for $\bar{P} = 0, \dots, P$, the probability that \bar{P} paths out of P are not detected $p_f(\bar{P})$ is given by:

$$p_f(\bar{P}) = \binom{L-P}{\bar{P}} \left(1 - p_c^{(L-P)}\right)^{\bar{P}} p_c^{(L-P)(P-\bar{P})}, \quad (25)$$

and $SNR_{\text{out}}^{(\bar{P})}$ is the corresponding output SNR given by:

$$SNR_{\text{out}}^{(\bar{P})} = SNR_{\text{in}} \frac{2M}{\frac{\mu(\sigma_f^2 \frac{P-\bar{P}}{P} + \psi^2)}{2 - \mu\psi^2} + 1} \frac{P - \bar{P}}{P}. \quad (26)$$

We assume for the sake of simplicity the case of an equal power partition over paths (*i.e.*, $\varepsilon_{p,n}^2 = 1/P$); hence the constant value of $p_c(\tau_p) = p_c$ in Eq. (25) and the fraction $(P - \bar{P})/P$ of signal power extracted from the detected paths in Eq. (26). In addition to this fraction, notice also the reduction of the identification errors term by the ratio P/L , compared to Eq. (23). This is due to the fact that only P vector fingers out of L are combined in the tracking mode in Eq. (11) after time-delay acquisition.

The resulting gain L/P in identification errors was also found in the less evident case of continuous time-delays addressed in [3], where even in the tracking mode all vector fingers are used. This shows that the projection of the estimated channel over a time manifold is the underlying reason for this gain (see [3]) and that the performance analysis holds whether the time-delays are multiples of T_c or continuous in $[0, T)$.

This reduction of identification errors improves the output SNR in the tracking mode despite the presence

of time-delay detection errors. Indeed, we noticed that SNR_{out}^T can be approximated by $SNR_{\text{out}}^{(0)}$ in very reasonable conditions. With $\mu \leq 0.05$ and $SNR_{\text{in}} \geq 0$ dB, $p_f(0)SNR_{\text{out}}^{(0)}$ is almost 44 dB above the sum of the remaining terms in Eq. (24). Fig. 4 plots the BER as a function of the input SNR with $\mu = 0.02$ and translates this improvement in SNR from the acquisition to the tracking mode into an enhancement in the BER, which was observed also in [3].

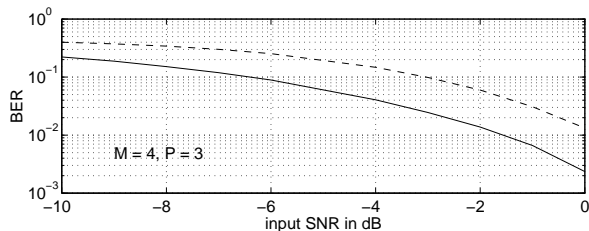


Figure 4 Experimental BER versus the input SNR after despreading in the acquisition (dashed) and the tracking (solid) modes for $\mu = 0.02$.

Now that we have established the advantage of the tracking mode, we can compute the capacity as a function of the required BER using their respective relations with the SNR given in [4]. We obtain the capacity C as a function of the BER value p_e after differential decoding of \hat{b}_n :

$$C(p_e) = \frac{L \left(\sqrt{1 + \frac{2MP\mu\psi^2(2-\mu\psi^2)}{[\text{erf}^{-1}(1-p_e)]^2}} - 1 \right)}{P\mu\psi^2(f+1)} + 1 \quad (27)$$

$$= \left(\frac{2ML}{(1+f)[\text{erf}^{-1}(1-p_e)]^2} + 1 \right) + O(\mu),$$

where $\text{erf}(x)$ is the usual error function [8] and f is a factor modeling the contribution of out-cell interference [1] (see [4] for more details).

As shown in Fig. 5, capacity increases with smaller values of μ and approaches the upper bound given in the second expression of Eq. (27) and established in [4], in the case of perfect channel identification and time-delay acquisition. This shows the impact of identification and synchronization errors on capacity.

With $M = 4$ antennas, $P = 3$ equal power paths and $f = 0.6$ (see [1],[4]), the capacity is upper bounded by 60 at a required BER of 10^{-3} and equal to 54, 57 and 58 with μ fixed at 0.04, 0.02 and 0.01, respectively. With $\mu = 0.01$ the loss in capacity is 3.3% compared to the upper bound. As we successively double the value of μ up to 0.02 and 0.04, we increase this loss by 1.7% and 6.7% respectively. However, we increase the speed of acquisition by 100% and 300% respectively.

Overall, STAR can achieve a high capacity [4] with a very fast and accurate time-delay acquisition.

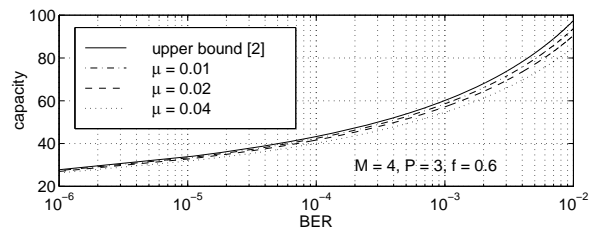


Figure 5 Static capacity in the tracking mode versus the required BER for different values of the step-size μ .

4. Conclusion

We analyzed in this paper the performance of STAR for cellular CDMA systems. We proved that STAR achieves very fast synchronization with a very small probability of false detection: with $M = 4$ antennas, $P = 3$ equal power paths and an input SNR around 0 dB, we can expect a time-delay acquisition with a probability of false detection as small as 10^{-6} within 10 bit iterations only. In addition, loss in capacity due to acquisition errors is relatively small.

References

- [1] A.J. Viterbi, *CDMA: Principles of Spread Spectrum Communication*, Addison-Wesley, 1995.
- [2] B. Suard, A.F. Naguib, G. Xu, and A. Paulraj, "Performance of CDMA mobile communication systems using antenna arrays", in *Proc. IEEE ICASSP'93*, vol. IV, pp. 153-156.
- [3] S. Affes and P. Mermelstein, "A new receiver structure for asynchronous CDMA : the spatio-temporal array-receiver (STAR)", *IEEE J. on Selec. Areas in Comm.*, to appear in the 3rd quarter of 1998.
- [4] S. Affes and P. Mermelstein, "Capacity improvement of cellular CDMA by the subspace-tracking array-receiver", in *Proc. IEEE SPAWC'97*, pp. 233-236.
- [5] B. H. Khalaj, A. Paulraj, and T. Kailath, "2D RAKE receivers for CDMA cellular systems", in *Proc. IEEE GLOBECOM'94*, vol. 1, pp. 400-404.
- [6] M.D. Zoltowski and J. Ramos, "Blind multiuser access interference cancelation for CDMA based PCS/cellular using antenna arrays", in *Proc. IEEE ICASSP'96*, vol. 5, pp. 2730-2733.
- [7] S. Haykin, *Adaptive Filter Theory*, Prentice-Hall, 1991.
- [8] J.G. Proakis, *Digital Communications*, McGraw-Hill, 1995.